Diffusion of 77 000 g/mol Dextran in Submicron Polyelectrolyte Capsule Dispersions Measured Using PFG-NMR

Thorsteinn Adalsteinsson,*,†,‡ Wen-Fei Dong,†,§ and Monika Schönhoff†,‡,||

Max Planck Institut für Kolloid und Grenzflächenforschung, Golm/Potsdam, D-14476, Germany, and Institut für Physikalische Chemie, Universität Münster, Correnstrasse 30, D-48149 Münster, Germany

Received: June 28, 2004; In Final Form: October 1, 2004

Pulsed field gradient NMR (PFG-NMR) spectroscopy is introduced to probe the distribution and dynamics of long dextran sugars (77 kDa) in heterogeneous solutions containing submicron hollow polymeric capsules. The capsules are made using the layer-by-layer (LBL) self-assembly method of strong polyelectrolytes onto silica microspheres, followed by a dissolution of the silica core. The resulting capsules are completely permeable for water and small ions, but large molecules, such as polydextran, are found to be in slow exchange between the capsule interior and the surrounding water. The spin−lattice relaxation time (T_1) for the aliphatic protons on the dextran is extracted from the variation of the apparent population of encapsulated dextran. The spin−spin relaxation time (T_2) of the encapsulated dextran is estimated by a combined diffusion−relaxation measurement. Both relaxation times are used to calculate the population of encapsulated dextran and to discuss the state of the encapsulated dextran. The NMR measurements here indicate that the dextran may preferentially select the capsule interior, resulting in an enriched dextran concentration inside the capsules. The encapsulated dextran appears to be in a liquidlike state rather than being immobilized on the capsule wall.

Introduction

Layer-by-layer (LBL) assembly of polyelectrolyte multilayers is a refined method for surface modification.[1−5] The architecture and function of the surface can be tailored by the choice of polyelectrolytes, either by the direct adsorption of a functional polymer to a surface[6] or by the subsequent modification of the adsorbed polymer.[7,8] The surface may in this way be tailored to act as a reactive site, or as a protective barrier for the substrate.[9] An attractive approach for maximizing the surface area is to use colloidal particles as substrates. In a new development for this field, the core colloid was successfully removed,[10] leaving only the hollow polyelectrolyte capsule in solution. This system has received increasing attention, as it may be both scientifically and technologically interesting. A variety of applications has been suggested, ranging from nonsurfactant emulsifiers[11] to microreactors[12,13] and drug delivery systems.[14,15] One of the key aspects of a hollow capsule is its permeability. This permeability is an interplay between the pore size, or the polymer network density, of the capsule wall and the specific interactions of the wall with the permeating molecule. A number of studies have focused on studying the permeability of fluorescent probe molecules into capsules, employing poly(allylaminhydrochloride)/poly(sodium styrene sulfonate) (PAH/PSS) capsules and poly(diallyldimethylammonium chloride)/PSS (PDADMAC/PSS) capsules.[12,16−21] These studies have been done using confocal microscopy imaging and basic fluorescence recovery after photobleaching (FRAP). One of the limitations when using microscopy is that the research can only be done on a very small number of selected capsules that are immobilized under the microscope. Furthermore, only dye-labeled probe molecules can be studied using this technique. The goal of the work presented here is to introduce pulsed field gradient nuclear magnetic resonance (PFG-NMR) spectroscopy for studying the dynamics of probe molecules in these submicron hollow capsule dispersions. In this way, we want to measure the ensemble average diffusion and distribution of nonfluorescing probe molecules in highly concentrated dispersions of capsules.

PFG-NMR spectroscopy is a powerful method for probing the structure of heterogeneous systems[22−24] and can, for example, probe the residence time of molecules in separate environments.[25−27] This technique has recently been applied successfully to study the permeation of small molecules through polymerized nanocapsules[28,29] and is also frequently used to study the diffusivity in dense gel systems and microemulsions.[30] The real power of PFG-NMR spectroscopy lies within the fact that practically any spin within a molecule can be used as a diffusion probe. Another power of the method is that, for a given spin, the probability function of the mean square displacement is measured directly for a fixed evolution time. This returns the average self-diffusion coefficient for various time or length scales. This evolution time, often called the diffusion time, can be varied from a few milliseconds to seconds, depending on the relaxation time of the spin. For example, for a spin that has a diffusion coefficient of 10^{-11} m^2/s, the accessible length scale in the PFG-NMR measurement is from several hundred nanometers to microns.

Here, hollow capsules that are small on the diffusion length scales were chosen. The assumption is that the capsules are truly hollow with a very thin wall in comparison with the diameter. A core material, or template, of submicron silica beads was chosen, since the silica can be completely removed by hydro-

* To whom correspondence should be addressed. E-mail: tadalste@mtholyoke.edu.
† Max Planck Institut für Kolloid und Grenzflächenforschung.
‡ Universität Münster.
§ E-mail: wenfei.dong@mpikg-golm.mpg.de.
|| E-mail: schoenho@uni-muenster.de.

10.1021/jp047208h CCC: $27.50
Published on Web 11/25/2004

fluoric acid once the capsule wall has been built up.[31] Polymeric template particles, such as melamin and polystyrene, may leave polymer oligomers upon dissolution that will affect the permeability of the capsule by partially rupturing the capsules.[21] The polyelectrolyte pair used here was PDADMAC/PSS because both polyelectrolytes are highly charged and insensitive to pH, salt, and other external factors. The diffusant was linear dextran polymer, which has been previously studied by confocal microscopy.[16] Dextran is uncharged at neutral pH and should therefore not adsorb to the capsule as a new molecular layer.

Materials and Methods

The water used here is purified through a Seradest USF 800 water purification system, with an initial resistivity of around 18 MΩ·cm. Deuterium oxide (99.9% isotopic purity) was purchased from Aldrich. Dextran (77.0 kDa, powder) and poly(diallyldimethylammonium chloride) (PDADMAC), M_w = 100 000−150 000 g/mol, were purchased from Aldrich and used without further purification. Poly(sodium-4-styrenesulfonate) (PSS) in powder form, M_w = 70 000 g/mol, was purchased from Sigma. The PSS was purified by filtration through a 20 μm filter, followed by dialysis against pure water (10 000 g/mol cutoff). Rhodamin-labeled PSS (TRIC-PSS) was prepared by free radical polymerization following a standard procedure described in the literature.[13] The synthesized polymer was purified by dialysis (M_w cutoff 12 000 g/mol) against pure water. A small amount of this polymer (0.2% w/w) was used in the preparation of the capsules in order to enable fluorescence imaging of the capsules and to verify the layer buildup in the preparation. Monodisperse silica particles with a radius of 260 nm were purchased from Geltech Inc. The powdered silica was dispersed in pure water and washed in centrifugation−decant−redispersion steps until the measured ζ-potential was stable and ~ -45 mV. Single particle light scattering (SPLS) was used to verify that the particles were monodisperse and not aggregated.

Capsule Formation. The polyelectrolyte multilayer capsules were prepared using a method previously described by Sukhorukov et al.[32] This method was further optimized for the use of small substrates by Schwarz and Schönhoff:[33] A silica colloid dispersion (2.5% w/v, salt-free) was added dropwise into a concentrated (1.5 mg/mL) polymer solution, containing 500 mM NaCl. The dilution of the NaCl concentration in the coating solution, which is due to the addition of the colloid dispersion, was compensated by simultaneous addition of concentrated (4 M) salt solution. The volume ratio between the colloid dispersion and the polymer solution was 1:5. After coating, the colloids were washed in centrifugation−decant−redispersion steps using pure water until the ζ-potential of the colloid dispersion reached a stable value and the resistivity of the decanted solution was in the MΩ·cm range. This process was repeated until four bilayers of PDADMAC/PSS were obtained.

The silica core was dissolved using dilute (0.50 M) hydrofluoric acid. The remaining capsules were washed in centrifugation−decant−redispersion steps until the pH of the decanted liquid was approximately 6 and no precipitates of CaF_2 were seen upon the addition of a $Ca(OH)_2$ solution. The degree of core removal was verified by atomic force microscopy (AFM) and SPLS. The volume fraction of the capsules in the samples reported here was based on the initial silica particle weight fraction of the colloid dispersion, assuming negligible losses of capsules during the core dissolution process. The approximate concentration can be verified by using SPLS.

Sample Preparation. To prepare samples for the NMR experiment, the water in the sample was exchanged for D_2O by six to seven washes similar to above, each time disposing ~95% of the supernatant. The mole fraction of H_2O to D_2O in the samples was measured as 0.16%. The samples used here are ≤10% v/v of 520 nm diameter capsules with 3.3 mg/mL dextran. The volume fraction of the capsules is based on the weight fraction of the colloid dispersion prior to core dissolution assuming negligible losses during centrifugation steps, which may be somewhat overestimated. The samples were stored for 2 days at room temperature prior to the measurements.

NMR Measurements. A Bruker 400 MHz Avance NMR spectrometer was used for the measurements. Relaxation measurements were taken on a liquid probe head using a deuterium lock. Diffusion measurements were done using a diffusion probe head (Bruker "Diff 30") fitted with a single 10 mm proton radio frequency (rf) coil. The maximum gradient strength obtained was 1200 G/cm. All measurements were done at room temperature (22.5 °C). The temperature of the gradient coils was held constant by a water circulation unit (Haake).

^{1}H Relaxation Measurements. The spin−lattice relaxation time (T_1) was measured by inversion recovery experiments [$\pi-\tau_1-{}^{\pi}/_{2}-$echo]. The spin−spin relaxation time (T_2) was measured by the Carr−Purcell−Meiboom−Gill (CPMG) sequence [${}^{\pi}/_{2}-(\tau_1-\pi-\tau_1)_n-$echo]. The delay time, here τ_1, was 2.0 ms.

^{1}H Pulsed Field Gradient NMR Measurements. The pulse program used here was the stimulated echo described by Stejskal and Tanner[34] in the sequence [${}^{\pi}/_{2}-\tau-{}^{\pi}/_{2}-T-{}^{\pi}/_{2}-\tau-$echo]. Two trapezoidal field gradient pulses of duration δ and strength g were applied following the first and third ${}^{\pi}/_{2}$ rf pulses. As a consequence of the pulse program, T_2 relaxation is active only during the delay time (τ). The spin lattice relaxation mechanism (T_1) is the only relaxation process active during the T delay. Hence, this sequence is well suited for polymers and larger molecules that have a relatively fast spin−spin relaxation rate.

The measured echo intensity for an isolated spin in a homogeneous system can, in the narrow pulse limit, be described by

$$I = \exp\left(\frac{-\Delta}{T_R}\right)\exp(-Dk) \tag{1}$$

where Δ is the diffusion time, T_R is the effective relaxation time, D is the self-diffusion coefficient, and k is given by

$$k = \gamma^2 g^2 \delta^2 (\Delta - \delta/3) \tag{2}$$

where γ is the gyromagnetic ratio of the nucleus, δ is the pulse duration, and g is the gradient strength. Δ is the diffusion time defined by the time between the two gradient pulses, here given by $\Delta = T + \tau$. In the following experiments, the gradient pulse length (δ) was varied between 1 and 2 ms and Δ was varied between 50 and 1000 ms. The measurements lie, therefore, in the narrow pulse limit in all cases. The effective relaxation time (T_R) is given by

$$\frac{1}{T_R} = \frac{1}{\Delta}\left(\frac{2\tau}{T_2} + \frac{T}{T_1}\right) \tag{3}$$

where τ and T are the two times in the pulse sequence.

In a system where a spin can exist in two separate environments, the most general description for the echo intensity decay

can be written as a superposition of two exponential functions,[25] or

$$I = P_A \exp(-a_A) + P_B \exp(-a_B) \quad (4)$$

where

$$a_{A,B} = \frac{1}{2}\left\{k(D_A + D_B) + \Delta\left(\frac{1}{T_B} + \frac{1}{T_A} + \frac{1}{\tau_B} + \frac{1}{\tau_A}\right) \mp \sqrt{\left[k(D_B - D_A) + \Delta\left(\frac{1}{T_B} - \frac{1}{T_A} + \frac{1}{\tau_B} - \frac{1}{\tau_A}\right)\right]^2 + \frac{4\Delta^2}{\tau_A \tau_B}}\right\} \quad (5)$$

Here, T_A and T_B are the effective relaxation times for the nucleus in sites A and B, respectively. Furthermore, τ_A and τ_B are the residence times for the nucleus in the different sites. The exponential prefactors are given by

$$P_B = 1 - P_A = \frac{1}{a_B - a_A}\left\{p_A\left(kD_A + \frac{\Delta}{T_A}\right) + p_B\left(kD_B + \frac{\Delta}{T_B}\right) - a_A\right\} \quad (6)$$

with

$$p_{A,B} = \frac{\tau_{A,B}}{\tau_A + \tau_B} \quad (7)$$

where p is the probability of finding a molecule in a given site. According to this description, a solution can be found for any combination of exchange, diffusion, and relaxation time scales. The limiting case of slow exchange, $\tau_{ex} \gg \Delta$, will be discussed in further detail in the Discussion section.

Results

Layer Formation and Preparation of Capsules. Whereas most work in the literature has been done using capsules several microns in diameter, the focus here is on capsules an order of magnitude smaller. Small capsules are a more suitable barrier system for the NMR diffusion measurements, since their size is small on the length scale of the measurements. However, smaller colloids are generally harder to use as substrates for multilayer buildup and the resulting layers are often viewed as being less stable. The success of the layer buildup is therefore demonstrated in the following section.

The inversion of surface charge is in agreement with previous experiments reported by Sukhorukov et al.[32] A small amount of TRIC-PSS was used in a mixture with unlabeled PSS in order to image the buildup using confocal microscopy. The submicron-sized colloids are seen only as small red dots in the viewing field when the sample is illuminated by green light. Comparison of the samples showed a stepwise, even increase in the fluorescence intensity with an increasing number of PSS layers. SPLS data also showed and increase in layer thickness with an increasing layer number, although these data were somewhat scattered. On average, the thickness of the four bilayers was ~10 nm.

The AFM imaging and electron microscopy (EM) of dried capsules (see Figure 1) was used to verify the core dissolution process. The capsules are around 520 nm in diameter, which agrees well with the size of the template silica particles. Since the capsules are in a dry state when imaged, they show a typical folding of the wall, which is also seen with larger capsules. The wall was estimated to be around 16 nm from the AFM images. No sign of residual silica was seen in any of the images, and relatively few capsules appeared to be ruptured (broken). The conclusion is then that the relatively aggressive dissolution of the core by HF does not disrupt the polyelectrolyte layers.

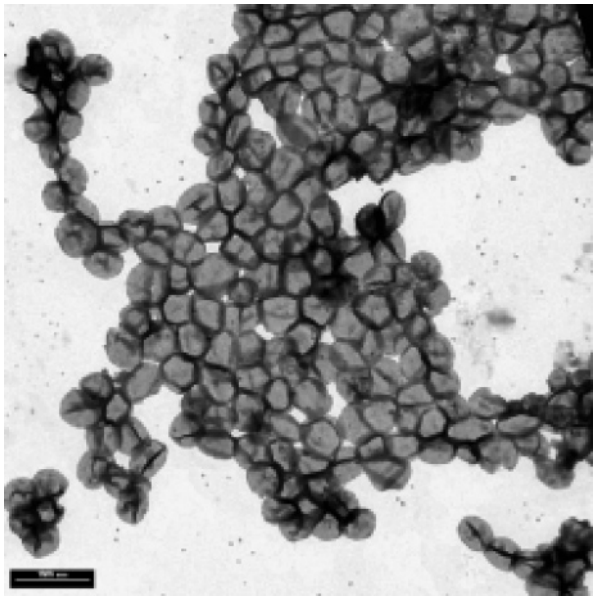

Figure 1. Electron micrograph of the capsules. The bar in the lower left corner is 1.0 μm. Ruptured capsules appear as fragments, or shapes with no signature of folding. Residual silica is normally seen as very dark round spots in the EM micrographs; folded or overlapping polyelectrolyte layers appear as dark shades.

Confocal imaging and SPLS measurements show that the capsules were somewhat aggregated. Approximately 75% of the capsules were singlets, doublets, and triplets. The remaining 25% were larger aggregates. Preventing aggregation of this kind is nearly impossible when a large quantity of particles is prepared with a high number of layers. The hollow capsules are easily dispersed in pure water and do not settle down to any significant extent over 48 h. This slow settling of the capsules is quite different from the behavior of larger capsules, which settle over a few hours. Only after sitting unperturbed for over a month, the small capsules settle down to a highly concentrated slurry, containing an ~15% volume fraction of capsules. Since the PFG-NMR diffusion measurements can take up to 4 h, this dispersion stability is a necessary requirement for the measurements here.

Adsorption of Dextran to the Capsules. To verify qualitatively that the dextran polymer does not permanently adsorb to the capsules, the following experiment was done using fluorescently labeled dextran (FITC-dextran). A drop of the capsule dispersion was allowed to stand on a poly(ethyleneimine) precoated microscope slide for a few minutes. A few of the negatively charged capsules adhere to the slide during this time. The excess solution and capsules were then rinsed off with water. Since the capsules are labeled with TRIC, they can be imaged as small red dots using green excitation light (Figure 2, A2). When the sample is excited by blue light (Figure 2, A1), very faint green dots are also seen due to the spectral overlap of the TRIC dye with blue light. Parts B1 and B2 of Figure 2 are taken of the same capsule-coated slide after allowing a solution of 3.3 mg/mL 66.1 kDa FITC-dextran to stand on the slide for an hour. After this time, the excess dextran was rinsed off and the pictures were taken. The prominent spots in parts B1 of Figure 2 reveal the position of the FITC dye. These spots overlap completely with the spots in part B2, which shows the position of the capsules. By repeated washing of the

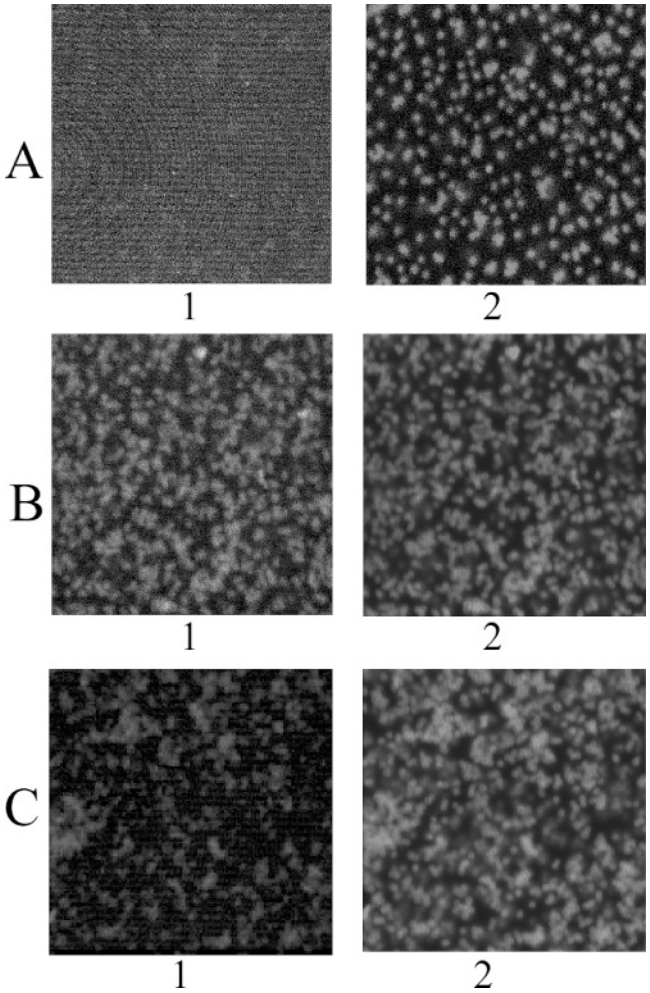

Figure 2. Confocal fluorescence images. Images A-1 and A-2 show capsule dispersion without FITC-dextran added. Images B-1 and B-2 show capsule dispersion after adding 66.1 kDa FITC-dextran and allowing it to stand for 1 h and then washing the excess dye off. Images C-1 and C-2 were taken after repeated washing of the sample in image B.

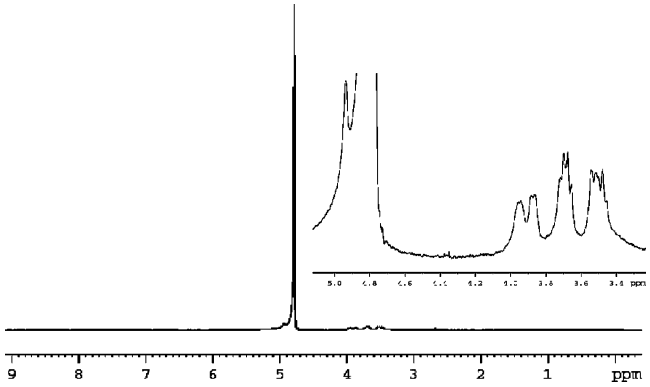

Figure 3. Proton NMR spectrum of 77 kDa FITC-dextran, 3.3 mg/mL. The inset shows an enlarged image of the aliphatic chains at 3.8 ppm. No signature of the FITC is visible in the spectrum.

slide with water, the intensity of the green spots could be reduced to near zero intensity (see part C1 of Figure 2) while the capsules remain on the slide (see part C2 of Figure 2). This experiment demonstrates that the dextran adheres or enters the capsules but is not permanently fixed to them.

NMR Measurements of Dextran in Pure D_2O and in a Capsule Dispersion. Figure 3 shows a typical NMR spectrum of 3.3 mg/mL 77 kDa dextran in D_2O. The peak at 4.8 ppm

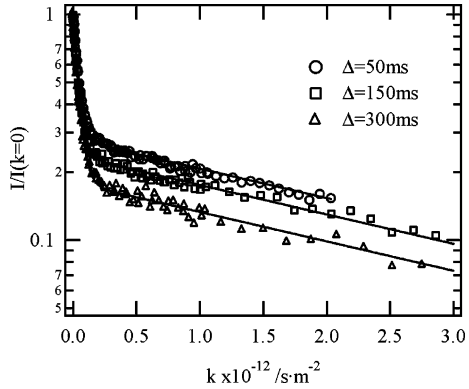

Figure 4. Plot of the echo intensity as a function of k. The three curves were collected using the three different diffusion times given in the legend. The spin−spin evolution time (τ in the pulse program) was fixed at 6.2 ms. The data were fitted using a double exponential decay function, $I = I_A \exp(-a_A k) + I_B \exp(-a_B k)$, and the fitting results are summarized in Table 1.

TABLE 1: Exponential Fitting Parameters from Figure 4

Δ/ms	$I_B = 1 - I_A$	$a_A/(m^2/s)$	$a_B/(m^2/s)$
50	0.360 ± 0.005	$(2.45 \pm 0.03) \times 10^{-11}$	$(3.56 \pm 0.16) \times 10^{-13}$
150	0.244 ± 0.004	$(2.45 \pm 0.04) \times 10^{-11}$	$(3.20 \pm 0.08) \times 10^{-13}$
300	0.193 ± 0.005	$(2.41 \pm 0.04) \times 10^{-11}$	$(3.32 \pm 0.13) \times 10^{-13}$

comes from residual water (HOD) in the solvent. The small shoulder in the water peak stems from alcohol protons on the dextran polymer. The peak series around 3.8 are the aliphatic protons on the dextran. These protons were chosen to monitor the diffusion behavior of the dextran, since the exchange between the alcohol protons and water may influence the apparent diffusion coefficient of the dextran.[35] The spectrum for the dextran in a capsule dispersion is similar.

Figure 4 shows three samples of Stejskal−Tanner plots of the dextran in the 10% v/v capsule dispersion. According to eq 1, the slope of the line is the negative diffusion coefficient. It is immediately apparent that two distinct populations of dextran exist in the dispersion. The three plots in the figure differ in the diffusion time (Δ) used in the experiment but use the same spin−spin relaxation evolution time ($\tau = 6.20$ ms) in the pulse sequence above. The diffusion times here are 50 ms (circles), 150 ms (squares), and 300 ms (triangles).

The solid lines in Figure 4 are fitted curves according to a double exponential fit, $I = I_A \exp(-a_A k) + I_B \exp(-a_B k)$. The fitting parameters from the double exponential fitting are shown in Table 1. The initial rapid decay of the echo intensity has an apparent diffusion coefficient of $a_A = (2.45 \pm 0.20) \times 10^{-11}$ m^2/s. This diffusion coefficient was found to be slightly slower than the diffusion coefficient for the dextran in pure D_2O, $(2.60 \pm 0.20) \times 10^{-11}$ m^2/s. This difference, although small, can be explained by free volume arguments using the capsule wall fraction (10%) as impermeable barriers to the free diffusion. The second apparent diffusion coefficient is $a_B = 3.3 \times 10^{-13}$ m^2/s. The size calculated for a spherical object with this diffusion coefficient, using the Stokes−Einstein theory, is nearly 750 nm, which is much greater than the size of the capsules. This diffusion coefficient agrees, however, with the diffusion coefficient of the capsules measured using dynamic light scattering (backscattered light). The observed diffusion behavior of the capsules is slower here than what is expected due to electrostatic repulsion between capsules at this high concentration.

The observation of a population of dextran molecules moving this slowly can be explained as follows: Assuming a Gaussian self-diffusion process of the dextran, each molecule would

sample a volume much larger than the volume of the capsules during the diffusion times used here. However, provided that the capsule wall acts as an impermeable barrier on the time scale (Δ), the dextran molecules cannot undergo a displacement that lies outside the capsule. The average position of a dextran molecule that is inside a capsule will therefore be at the center of the capsule, and the mean square displacement must be that of the capsule itself. On the basis of this, the two populations of the dextran are labeled as free and encapsulated, respectively, from their apparent diffusion coefficients. It is not clear at this point if the encapsulated dextran here is truly inside the capsules or rather adsorbed to the surface of the capsules. In the case of adsorption, one would however expect a rapid quenching of the NMR signal from this fraction, since relaxation processes of immobilized molecules are much more rapid than those of molecules in solution.

The variation of the apparent diffusion coefficients a_A and a_B with diffusion time (Δ) was found to be insignificant in comparison with the experimental error (see Table 1). This allows all the curves to be fitted reasonably using two universal diffusion coefficients. The only variable between curves from different measurements is therefore the intensity of the encapsulated fraction, here called I_B. The invariance of the apparent diffusion coefficients with Δ implies that the two populations of dextran in the sample are in a slow exchange between the two environments compared to the diffusion time, or $\Delta/\tau_{ex} \ll 1$, where τ_{ex} is the exchange time scale.

Extraction of Mole Fraction and Relaxation Rates. The intensity (I_B) can be related to the probability of finding a molecule encapsulated, or in other words, the mole fraction in site B. This can be extracted by using the intermediate exchange model by Kärger[25] in eq 4 above. In the slow exchange limit, the model can be simplified to

$$I = I_A \exp(-D_A k) + I_B \exp(-D_B k) \tag{8}$$

where $I_A + I_B = 1$. The parameter I_B contains the spin−spin and spin−lattice relaxation influence on the signal as well as the population of the encapsulated fraction. I_B can be written as $I_B = 1/(1 + E)$, where

$$E = \frac{p_A}{p_B} \exp\left(-\Delta\left(\frac{1}{T_A} - \frac{1}{T_B}\right)\right) \tag{9}$$

Using the definitions for the effective relaxation rates T_A and T_B given in eq 3 along with the identity from the pulse sequence that $T = \Delta - \tau$, one can write E in the form

$$E = \xi \exp(-\Delta\Omega) \tag{10}$$

with

$$\Omega = \frac{1}{T_{1A}} - \frac{1}{T_{1B}} \tag{11}$$

and

$$\xi = \frac{p_A}{p_B} \exp\left\{-\tau\left[2\left(\frac{1}{T_{2A}} - \frac{1}{T_{2B}}\right) - \Omega\right]\right\} \tag{12}$$

Using these equations, it is now possible with few assumptions to extract the true mole fractions, or probabilities (p_A and p_B), of free and encapsulated dextran along with the relaxation times T_{1B} and T_{2B} for the encapsulated fraction. To do so, an assumption is made that the relaxation time for fraction A is that of free dextran in D_2O, which can be measured separately.

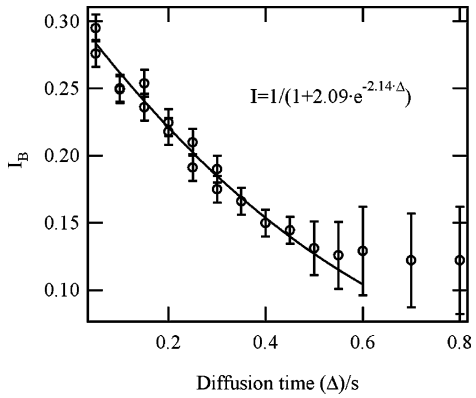

Figure 5. Plot of the intensity of slow moving molecules as a function of diffusion time. The spin−spin evolution time (τ in the pulse program) was fixed at 6.20 ms for all the measurements. The data were fitted according to the theory discussed in the text using $I = 1/(1 + E)$, where $E = \xi \exp(-\Delta\Omega)$.

Spin−Lattice Relaxation Time. According to this slow exchange model, the variation of I_B with diffusion time (Δ) seen in Figure 4 must arise from the difference in the T_1 relaxation time from one site to another. A set of measurements was therefore done where the diffusion time (Δ) was varied and the spin−spin evolution time (τ) was kept constant at 6.20 ms. Each of the resulting echo decays was fitted by using the known diffusion coefficients for each fraction as discussed earlier and by only varying I_B between echo curves. The resulting encapsulated fraction intensities along with the fitted line according to the model are shown in Figure 5. The range of Δ is limited to ~0.8 s by the T_1 relaxation time for the encapsulated dextran. At longer Δ, the signal intensity from this population was very low and the data points were scattered. Since the fitting procedure does not account for negative values of intensity, a systematic error is built up at these low intensities. Therefore, these curves were not fitted successfully using the model and the points were omitted from the fitted line in the figure. Using the relaxation time for dextran in pure D_2O, $T_{1A} = 1.040 \pm 0.020$ s, it is straightforward to extract the spin−lattice relaxation time for the encapsulated dextran, $T_{1B} = 0.322 \pm 0.020$ s.

The spin−lattice relaxation rate depends primarily on fast motion in molecules, such as rotation around a bond. In the case of dipolar nuclei, the relaxation also depends on the amount and strength of dipolar coupling of the spin with neighboring spins. This complicates the interpretation of proton relaxation rates, since it is in fact concentration dependent. The difference seen here in T_{1A} and T_{1B} is therefore either due to the binding of dextran, cross-polarization of protons in dextran with protons in the capsules, or higher concentration of dextran protons inside or on the capsules.

Spin−Spin Relaxation Time. The evaluation of the spin−spin relaxation is somewhat more complicated to do from the fit in Figure 5. The ξ value extracted from the fit includes the difference in both the spin−spin relaxation rates and the mole fractions in either of the sites (p_A and p_B). The relaxation time for the dextran in D_2O (T_{2A}) was measured as 0.113 ± 0.018 s, which is an order of magnitude smaller than T_{1A}. This is a common observation for the relaxation behavior of long molecules, since T_2 is influenced by slow motions of the spin, that is, the molecular tumbling rate and chain reorientation, whereas T_1 is not. Interestingly, relaxation measurements for T_2 of the dextran in the capsule dispersion, using a CPMG pulse sequence, returned almost the same value as that for the free dextran (T_{2A}). This may be an indication that T_{2B} is either very short or nearly identical to T_{2A}. We can argue against the case

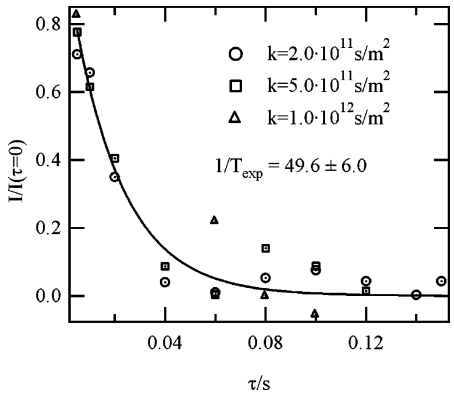

Figure 6. Hahn-echo experiment using a diffusion coefficient selection. The graph shows data for decay intensity at three different wave vectors at a diffusion time of 150 ms. The signal intensity is normalized to the extrapolated value at $\tau = 0$. At this high diffusion vector, only the encapsulated dextran contributes to the echo intensity. The fit in the figure is according to a single exponential decay function.

of extremely short T_{2B}. A short T_{2B} would have lead to little or no intensity of the encapsulated fraction in the diffusion measurement, since the total delay time (τ) where the T_2 relaxation process is dominating was 12.4 ms (2×6.20 ms). Furthermore, since the delay time in the CPMG measurement was very short (2 ms) and the molecules are in a slow exchange between the two environments, the echo should have been biexponential. If T_{2A} and T_{2B} are similar, the echo decay from the CPMG measurement is well described by a single exponential decay.

T_{2B} can be measured separately in an independent measurement using the PFG-NMR method once the value for T_{1B} is known. By selecting a fixed and high value for k, the signal arising from the fast moving molecules can be neglected, since this part decays rapidly (see Figure 4). By varying τ and keeping Δ fixed, the $\exp(-\Delta\Omega)$ term in eq 10 is held constant. Variation in I_B is then due to changes in the ξ term. Since the diffusion measurement selects a signal arising from the encapsulated dextran, the T_{2A} and T_{1A} terms in eqs 11 and 12 vanish. This experiment is effectively a Hahn-echo measurement of a population, selected by its diffusion coefficient. The simplicity of this approach rests on the assumption that the molecules are in a slow exchange in comparison to the diffusion time.

The results from this experiment are shown in Figure 6 for three different values of k, 2×10^{11}, 5×10^{11}, and 1×10^{12} s/m^2, for a fixed Δ value of 150 ms. The decays are normalized to a value extrapolated to $\tau = 0$. The fit appears to be a simple exponential decay, although the data points are somewhat scattered. The exponential decay time here is $1/T_{exp} = [(2/T_{2B}) - (1/T_{1B})]$, as was discussed above. Given that the value for T_{1B} is 0.322 s, it is simple to extract a value for T_{2B} of 0.038 ± 0.008 s.

While this value for T_{2B} is plausible, there is a large scattering of the data points in Figure 6. This scattering could be a result of the spins being J-coupled in the measurement rather than a pure signal/noise error. In fact, Hahn-echo measurements of the dextran in pure D_2O gave an oscillating echo intensity profile. If this decay was fitted using a simple exponential function, the relaxation time was 0.044 ± 0.011 s. In comparison, the value extracted using the CPMG pulse program was 0.113 ± 0.018 s, as reported above. Therefore, the value obtained for T_{2B} from Figure 6 can only serve as the lower limit for the real T_{2B}. The longest time for T_{2B}, assuming that motional restriction would reduce the T_2 value, is then that of T_{2A}, or in short, $0.038 \text{ s} < T_{2B} < 0.113$ s.

TABLE 2: Summary of Relaxation Times and Population Distribution

	outside capsules (A)	encapsulated (B)
T_1/s	1.040 ± 0.020	0.322 ± 0.020
T_2/s	0.113 ± 0.018	$0.038 \pm 0.005 < T < 0.113 \pm 0.018$
p/%	$68 < p_A < 63$	$32 < p_B < 37$

Mole Fraction of Encapsulated Dextran. Using this range of T_{2B} values in eq 10 along with the other relaxation times, summarized in Table 2, gives a range of $1.70 < p_A/p_B < 2.1$. This gives a mole fraction of encapsulated dextran of $32\% < p_B < 37\%$, which is an astonishing result, considering that the volume fraction of the capsules in the sample was only 10%. In other words, the dextran concentration inside the capsules is approximately 4 times higher than that outside the capsules.

Discussion

Two main questions should stand out at this point. The first is in regard to the state of the slow moving dextran in the capsule dispersion. Two possibilities are considered. The dextran could be adsorbed to the capsule or encapsulated inside. The second question is in regards to the physical reasons for the enrichment observed.

Nothing in the confocal microscopy experiments with the dextran indicated that it adsorbed strongly to the charged surfaces that were used. The bright FITC-dextran intensity was in fact mostly washed away with repeated washes using pure water. This is somewhat expected, since dextran has no charge and is highly hydrated.

Spin relaxation times are commonly used to determine the immobilization of molecules.[36−39] Proton relaxation rates are rarely used for this purpose, since the relaxation rate depends on the coupling strength and the number of coupling of the relaxing spin with its neighboring spins. In addition to this coupling, spin−lattice relaxation is only sensitive to motions of the spin with a frequency close to the Larmor frequency. Typical for these types of motions are bond rotations, which are not restricted by the immobilization of molecules to fluid layers, gels,[40] or fluid micelles.[37] Spin−spin relaxation rates are in addition dependent on slow motions of the molecule, such as rotational tumbling. Adsorption will change this tumbling dramatically, and therefore, the T_2 relaxation time is commonly expected to drop by one or more orders of magnitude upon immobilization.

The difference measured here in T_{1A} and T_{1B} of a factor of 3 is somewhat larger than expected. This difference indicates either that extreme restriction occurs of the aliphatic protons in the dextran when encapsulated or that the number of coupling spins is higher for the encapsulated fraction. Strong binding should reduce the spin−spin relaxation time much more dramatically, which is not observed. Instead, the maximum difference in T_{2A} and T_{2B} is approximately a factor of 3 as well.

This agreement of a factor of 3 is an indication that the proton density surrounding the relaxing aliphatic protons is much higher inside the capsules than in pure D_2O. This is again in agreement with the observation made in the last paragraph of the last section that the dextran concentration is indeed higher in the capsules than outside the capsules. In summary, the relaxation times demonstrate that the dextran is not predominately in an immobile state, as a gel or adsorbed layer, when encapsulated.

The preparation of the samples dictates that the maximum volume fraction of capsules in the sample is 10% of the total volume of the solution. This fraction is based on the weight fraction of the coated silica particles prior to the HF treatment.

The true volume fraction is probably less than this due to losses of capsules during the sample preparation. The mole fraction of encapsulated dextran measured is ~30−40%. Since the average concentration of dextran in the sample is known (3.33 mg/mL), the inside concentration is around 10−15 mg/mL at equilibrium. This concentration is close to the overlap concentration of this size dextran.

What has not been discussed so far is the influence that the capsule wall has on the dextran. While the polyelectrolytes are extremely water soluble in their fully charged state, the complex that is formed when polycations and polyanions are mixed is insoluble in pure water. This is due to the complexation of multiple positive and negative ions along the polymer backbone. Despite this, the polyelectrolytes are strongly hydrated and very polarizable. To a first approximation, the $(PDADMAC/PSS)_4$ capsule wall used here can be considered as a 10 nm thick uncharged hydrated polymer matrix, that is negatively charged toward the outside solution and positively charged toward the inside solution. It has been hypothesized[41,42] that the positive polyelectrolyte has a stronger bound hydration shell around it than the negative polyelectrolyte. The result may be that the positive charges on the inside of the capsule build up a dextran shell around them in order to screen away the nearby charges. The loss of entropy of the dextran is compensated by an increase in entropy of the freed up hydration water in the positive polymer layer. There may also be an enthalpic contribution favoring this binding, since each dextran monomer has multiple polarizable oxygen atoms. Due to the size of the dextran, this adsorbed layer is likely to be entangled. Dextran inside this thin entangled layer has a lowered probability of escaping the capsule, since this fraction has to permeate through both the dextran layer and the capsule wall. Dextran entering the capsule through the polymer matrix can on the other hand replace the pre-existing layer. At equilibrium, the number of dextran molecules escaping the capsule must equal the number of molecules entering the capsule, and since the rate of escaping is lower than the rate of entering, the concentration inside must be higher than that outside. The thin entangled layer of dextran is less likely to form on the outside of the capsule, since each sugar ring on the dextran does not have acidic protons or amine groups that can stabilize a negative charge.

Conclusions

Here, pulsed field gradient NMR spectroscopy was successfully used on polyelectrolyte capsule dispersions for the first time. The requirement for this was mainly that the capsules stay dispersed during the measurement and that the probe molecule does not adsorb irreversibly to the capsule. Furthermore, a high amount of capsules is required for a sufficient signal.

The first observation of interest in this work is that the exchange between the capsule interior and the capsule exterior is slow on the time scale of the PFG-NMR measurement. Here, the measurements were done between 10 and 600 ms. The hypothesis that the dextran is not permanently adsorbed to the capsule from confocal examination is backed up by the NMR observations that the dextran is not in a crystalline or solid form.

A slow exchange model derived from Kärger's intermediate exchange model enables us to extract the relaxation times of the dextran fraction here referred to as encapsulated, rather than adsorbed. At this point, we have no solid evidence that the dextran is indeed found in the interior of the capsule, or if it is only weakly bound to the capsule wall with a slow exchange time scale. The arguments in the Discussion section point toward a conclusion that the difference in the relaxation times can be explained from the concentration difference, and hence, the encapsulation idea is enforced.

Perhaps the most interesting of the results here is the fraction of the encapsulated dextran in the system. The physical reason for this enrichment is not clear at this point either. A working hypothesis is that the dextran adsorbs first weakly to the capsule wall interior, generating an entangled corona on the capsule interior. This corona then restricts the probability of a molecule further inside the capsule from leaving the capsule. This growth, or entanglement, reaches equilibrium where the concentration inside the capsule has to be 4 times higher than that outside the capsule.

Acknowledgment. The authors thank Olaf Niemeyer and Annegret Praast for technical assistance as well as Helmuth Möhwald for fruitful discussions and support of this project.

References and Notes

(1) Decher, G.; Hong, J. D.; Schmitt, J. *Thin Solid Films* **1992**, *210*, 831.
(2) Lvov, Y.; Decher, G.; Möhwald, H. *Langmuir* **1993**, *9*, 481.
(3) Chen, W.; McCarthy, T. J. *Macromolecules* **1997**, *30*, 78.
(4) Schönhoff, M. *J. Phys.: Condens. Matter* **2003**, *15*, R1781.
(5) Schönhoff, M. *Curr. Opin. Colloid Interface Sci.* **2003**, *8*, 86.
(6) Cheung, J. H.; Fou, A. F.; Rubner, M. F. *Thin Solid Films* **1994**, *244*, 985.
(7) Jiang, X. P.; Hammond, P. T. *Langmuir* **2000**, *16*, 8501.
(8) Lee, S. H.; Balasubramanian, S.; Kim, D. Y.; Viswanathan, N. K.; Bian, S.; Kumar, J.; Tripathy, S. K. *Macromolecules* **2000**, *33*, 6534.
(9) Elbert, D. L.; Herbert, C. B.; Hubbell, J. A. *Langmuir* **1999**, *15*, 5355.
(10) Donath, E.; Sukhorukov, G. B.; Caruso, F.; Davis, S. A.; Möhwald, H. *Angew. Chem., Int. Ed.* **1998**, *37*, 2202.
(11) Moya, S.; Sukhorukov, G. B.; Auch, M.; Donath, E.; Möhwald, H. *J. Colloid Interface Sci.* **1999**, *216*, 297.
(12) Sukhorukov, G. B.; Brumen, M.; Donath, E.; Möhwald, H. *J. Phys. Chem. B* **1999**, *103*, 6434.
(13) Dähne, L.; Leporatti, S.; Donath, E.; Möhwald, H. *J. Am. Chem. Soc.* **2001**, *123*, 5431.
(14) Choi, S. W.; Kim, W. S.; Kim, J. H. *J. Dispersion Sci. Technol.* **2003**, *24*, 475.
(15) Pastoriza-Santos, I.; Schöler, B.; Caruso, F. *Adv. Funct. Mater.* **2001**, *11*, 122.
(16) Antipov, A. A.; Sukhorukov, G. B.; Leporatti, S.; Radtchenko, I. L.; Donath, E.; Möhwald, H. *Colloids Surf., A* **2002**, *198*, 535.
(17) Dai, Z. F.; Dähne, L.; Möhwald, H.; Tiersch, B. *Angew. Chem., Int. Ed.* **2002**, *41*, 4019.
(18) Ge, L. Q.; Möhwald, H.; Li, J. B. *Biochem. Biophys. Res. Commun.* **2003**, *303*, 653.
(19) Glinel, K.; Sukhorukov, G. B.; Möhwald, H.; Khrenov, V.; Tauer, K. *Macromol. Chem. Phys.* **2003**, *204*, 1784.
(20) Ibarz, G.; Dähne, L.; Donath, E.; Möhwald, H. *Chem. Mater.* **2002**, *14*, 4059.
(21) Ibarz, G.; Dähne, L.; Donath, E.; Möhwald, H. *Macromol. Rapid Commun.* **2002**, *23*, 474.
(22) Callaghan, P. T.; Coy, A.; Halpin, T. P. J.; Macgowan, D.; Packer, K. J.; Zelaya, F. O. *J. Chem. Phys.* **1992**, *97*, 651.
(23) Callaghan, P. T. *J. Magn. Reson., Ser. A* **1995**, *113*, 53.
(24) Lindblom, G.; Orädd, G. *Prog. Nucl. Magn. Reson. Spectrosc.* **1994**, *26*, 483.
(25) Kärger, J. *Adv. Colloid Interface Sci.* **1985**, *23*, 129.
(26) Schönhoff, M.; Södermann, O. *J. Phys. Chem. B* **1997**, *101*, 8237.
(27) Schönhoff, M.; Södermann, O. *Magn. Reson. Imaging* **1998**, *16*, 683.
(28) Mayer, C.; Hoffmann, D.; Wohlgemuth, M. *Int. J. Pharm.* **2002**, *242*, 37.
(29) Wohlgemuth, M.; Mayer, C. *J. Colloid Interface Sci.* **2003**, *260*, 324.
(30) Griffiths, P. C.; Cheung, A. Y. F.; Davies, J. A.; Paul, A.; Tipples, C. N.; Winnington, A. L. *Magn. Reson. Chem.* **2002**, *40*, S40.
(31) Dai, Z. F.; Möhwald, H.; Tiersch, B.; Dähne, L. *Langmuir* **2002**, *18*, 9533.
(32) Sukhorukov, G. B.; Möhwald, H.; Decher, G.; Lvov, Y. M. *Thin Solid Films* **1996**, *285*, 220.
(33) Schwarz, B.; Schönhoff, M. *Colloids Surf., A* **2002**, *198*, 293.

(34) Tanner, J. E.; Stejskal, E. O. *J. Chem. Phys.* **1968**, *49*, 1768.
(35) Cabrita, E. J.; Berger, S. *Magn. Reson. Chem.* **2002**, *40*, S122.
(36) Nydèn, M.; Söderman, O.; Hansson, P. *Langmuir* **2001**, *17*, 6794.
(37) Schönhoff, M.; Söderman, O. *J. Phys. Chem. B* **1997**, *101*, 8237.
(38) Wiedmer, S. K.; Riekkola, M. L.; Nydèn, M.; Söderman, O. *Anal. Chem.* **1997**, *69*, 1577.
(39) Stubenrauch, C.; Nyden, M.; Findenegg, G. H.; Lindman, B. *J. Phys. Chem.* **1996**, *100*, 17028.
(40) Naji, L.; Schiller, J.; Kaufmann, J.; Stallmach, F.; Kärger, J.; Arnold, K. *Biophys. Chem.* **2003**, *104*, 131.
(41) Schwarz, B.; Schönhoff, M. *Langmuir* **2002**, *18*, 2964.
(42) Carrière, D.; Krastev, R.; Schönhoff, M. *Langmuir*, in press, 2004.